On-Demand Delivery of Single DNA Molecules Using Nanopipets

Aleksandar P. Ivanov,[*,†,⊥] Paolo Actis,[‡,⊥] Peter Jönsson,[§,∥,⊥] David Klenerman,[∥] Yuri Korchev,[‡] and Joshua B. Edel[*,†]

[†]Department of Chemistry, Imperial College London, London SW7 2AZ, United Kingdom, [‡]Department of Medicine, Imperial College London, London W12 0NN, United Kingdom, [§]Department of Chemistry, Lund University, Lund SE-221 00, Sweden, and [∥]Department of Chemistry, University of Cambridge, Cambridge CB2 1EW, United Kingdom. [⊥]A.P.I., P.A., and P.J. contributed equally to this work.

ABSTRACT Understanding the behavioral properties of single molecules or larger scale populations interacting with single molecules is currently a hotly pursued topic in nanotechnology. This arises from the potential such techniques have in relation to applications such as targeted drug delivery, early stage detection of disease, and drug screening. Although label and label-free single molecule detection strategies have existed for a number of years, currently lacking are efficient methods for the controllable delivery of single molecules in aqueous environments. In this article we show both experimentally and from simulations that nanopipets in conjunction with asymmetric voltage pulses can be used for label-free detection and delivery of single molecules through the tip of a nanopipet with "on-demand" timing resolution. This was demonstrated by controllable delivery of 5 kbp and 10 kbp DNA molecules from solutions with concentrations as low as 3 pM.

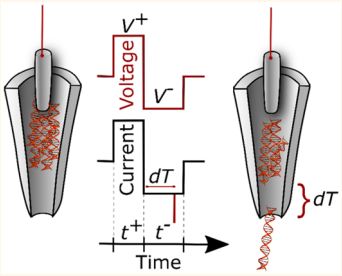

KEYWORDS: single-molecule delivery · label-free detection · nanopore · nanopipet · DNA

Rapid single-molecule detection and controllable single-molecule delivery are two of the central themes of modern nanotechnology. Unfortunately these themes are often disconnected, particularly in environments which require physiological and label-free conditions. A class of versatile single-molecules detectors, nanopores or nanopipets, has shown exceptional promise for label-free analysis of key life components such as DNA, RNA, and proteins[1−10] but has not been used for controllable delivery of biomolecular species. The ability to simultaneously deliver and analyze individual molecules in label-free conditions is one of the ultimate goals in nanotechnology and can open up avenues for the quantitative analysis of biological, chemical, and physical phenomena on an individual nonstatistical basis. However, at the single molecule level, the analyte transport (and detection) across the nanopore is typically a random process, resulting in limited control on the transport of individual molecules.

In a typical nanopore sensing platform, two reservoirs containing electrolyte are connected via a nanoscale pore. Voltage is applied across the nanopore to generate a steady-state ionic current that depends on the pore dimensions, charge, and the ionic strength of the solution.[1,3] Analytes are electrokinetically translocated through the nanopore and are detected by transient variations in the ionic current. A subclass of nanopores, used in this work, is nanopipets. Importantly, they can be rapidly and inexpensively laser pulled from glass capillaries, resulting in a sharp tip constituting a single nanopore, which can be used as single-molecule label-free sensors,[10−14] in the same way as conventional solid-state nanopores. Because of their high-aspect ratio geometry and exceptionally sharp tips, nanopipets offer an important advantage over conventional nanopores as they can be easily adapted for use in single cell interrogation[15,16] and as a macroscopic delivery vehicle for intracellular injection.[17−22] To date, delivery of molecules has so far only been quantified in close proximity to the tip by using fluorescence spectroscopy.[18,21,23] Real-time quantitative delivery of *individual molecules* combined with label-free nanopore detection has yet to be achieved. In fact nanopipets are predominantly used as an analytical platform for the detection of single molecules by transporting molecules from the outside reservoir to the inside of the nanopipet.[10,12,13,24−27] However, this

* Address correspondence to aivanov@imperial.ac.uk, joshua.edel@imperial.ac.uk.

Received for review February 8, 2015 and accepted March 20, 2015.

Published online March 20, 2015
10.1021/acsnano.5b00911

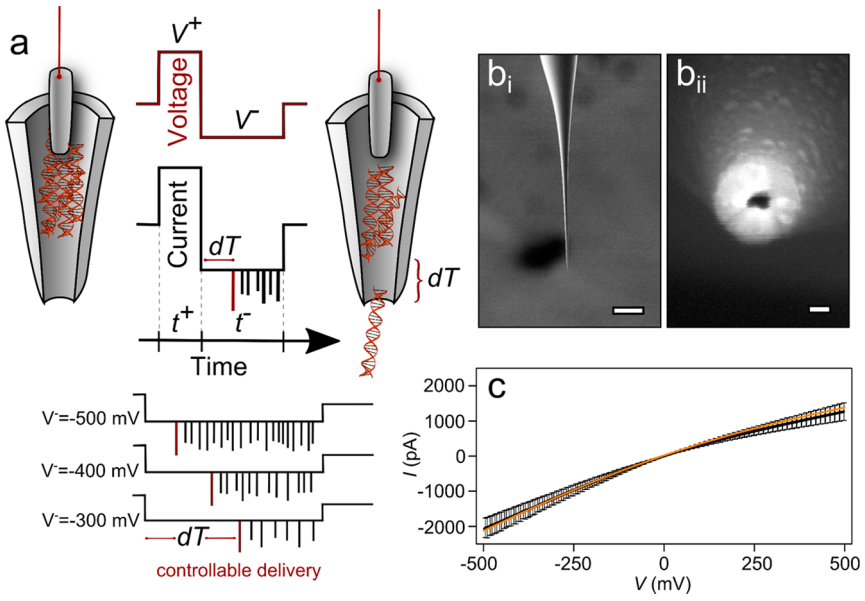

Figure 1. Controlled delivery with a nanopipet: (a) schematic illustration showing the nanopipet delivery system. Positive (V^+) and negative (V^-) voltage pulses are applied for t^+ and t^-, respectively. Single DNA molecules are delivered during a (V^-) pulse and are detected as transient changes in the ion current. (b) SEM images of the nanopipet tip (b_i) and the nanopore at the tip (b_{ii}). The scale bars are 250 μm and 25 nm, respectively. The nanopipets had an inner half-cone angle of θ = 3.5° resulting in a high length to width ratio of the nanopipet tip. (c) Average $I-V$ curves of 10 nanopipets measured in 0.1 M KCl (black). The average ionic resistance was R = 250 ± 35 MΩ. All nanopipets exhibited ion current rectification with a ratio I_{-500mV}/I_{500mV} = 1.6 ± 0.4. The orange line is an $I-V$ curve calculated by finite element simulations in COMSOL Multiphysics by modeling the electric field, ion current, and electroosmotic flow in the nanopipet as described in the Methods section. The simulated rectification ratio is I_{-500mV}/I_{500mV} = 1.5.

does not take advantage of utilizing the nanopipet as a label-free single-molecule delivery vehicle.

Here, we address this fundamental gap and report on simultaneous label-free detection and on-demand delivery of single DNA molecules with nanopipets, with precise control of the time of delivery and the number of delivered molecules. Molecular delivery is demonstrated down to picomolar concentrations (<10^6 DNA molecules in submicroliter volumes), advancing high-sensitivity detection and delivery of unamplified samples using nanopipets. Additionally, molecules can be controllably transported back and forth prior to reaching the tip of the nanopipet by using asymmetric voltage pulses, acting as an "on−off switch" for on-demand molecular delivery. Ultimately, we envision applications in controllable delivery of individual oligonucleotides (inside living cells), providing new insights in processes such as gene regulation and infection and single-molecule PCR, to mention a few examples.

RESULTS AND DISCUSSION

A schematic of the principle behind the experiment is shown in Figure 1a. Quartz nanopipets were fabricated by laser-assisted pulling as described in the Methods section. The nanopipets used in this study had a resistance of 250 ± 35 MΩ (as measured in a low bias (−0.1 V; 0.1 V) regime in 0.1 M KCl, 10 mM Tris/EDTA, pH 8) and a nanopore diameter of 25 ± 4 nm, as determined by SEM (Figure 1b). All nanopipets exhibited I_{-500mV}/I_{500mV} = 1.6 ± 0.4 (Figure 1c), consistent with the rectification behavior observed in negatively charged conical geometries.[28−31]

The nanopipets were filled with (5 kbp or 10 kbp) double-stranded DNA solution and Ag/AgCl electrodes were fitted both in the nanopipet (patch electrode) and in the external reservoir containing only buffer (bath/ground electrode). Under these conditions, the negatively charged DNA molecules inside the nanopipet migrate toward the inner electrode under positive applied potentials and toward the tip of the nanopipet under negative potentials. In contrast to traditional nanopore experiments where a constant dc voltage is applied, we used periodic pulses of positive (V^+) and negative (V^-) potentials with durations t^+ and t^-, respectively. This allowed us to minimize clogging of the nanopipet[32] and, importantly, to deliver individual DNA molecules through the tip of the nanopipet in a controllable manner (schematic Figure 1a). We observed that in each pulse, the time between the application of V^- and the detection of the first translocation event (dT) was remarkably regular and could be controlled by varying the magnitude of V^-, V^+, and t^+. Figure 2a shows representative time traces for voltage ($V-t$) and current ($I-t$) during 500 s (24 consecutive delivery pulses) for delivery from one of the DNA solution used (150 pM, 10 kbp DNA). During a V^- pulse, individual DNA molecules are delivered and detected as transient changes of the ionic current as shown in Figure 2b (zoomed in views of several representative

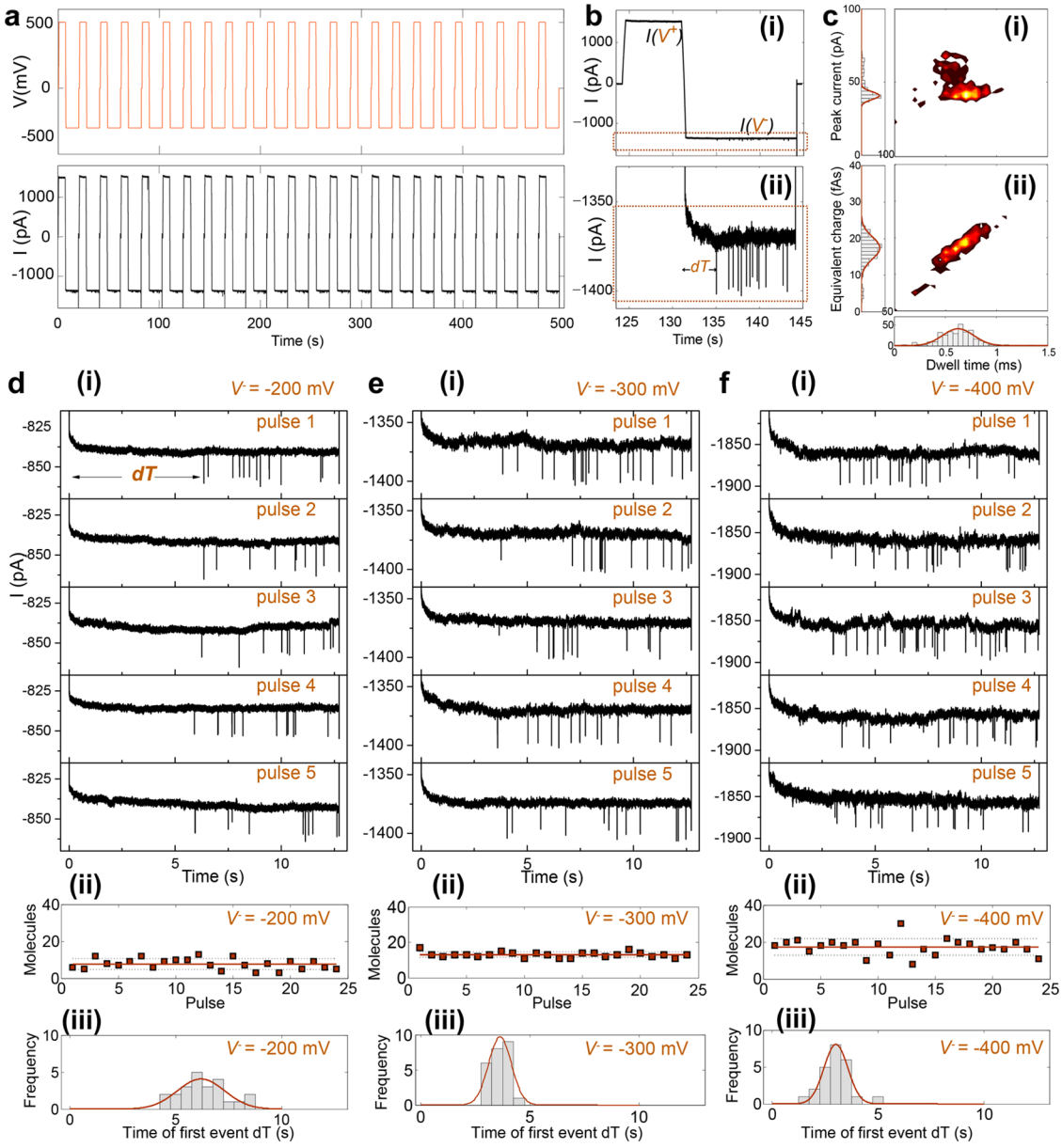

Figure 2. Single molecule detection and delivery. (a) $I-t$ and $V-t$ measurements of the first 500 s (24 delivery cycles) of 150 pM, 10 kbp DNA molecules, with $V^+ = 500$ mV, $V^- = -300$ mV, $t^+ = 6.4$ s, and $t^- = 12.7$ s. (b, i) A magnified view of a single cycle showing the $I-t$ trace for V^+ and V^- pulses and (ii) and a magnified view of the same current trace for V^- showing individual delivery events. (c, i) Event scatter plots of peak current (after baseline subtraction) versus dwell time and (ii) equivalent charge vs dwell time for the 24 cycles show in part a. At $V^- = -300$ mV, the most probable pore dwell time is 0.6 ± 0.2 ms with a mean charge (integrated current area per translocation) of 18.0 ± 4.1 fAs, as calculated from the histogram fits. d,e,f (i) Representative $I-t$ traces for delivery of 150 pM, 10 kbp DNA for $V^- = -200$ mV, $V^- = -300$ mV, and $V^- = -400$ mV, respectively. For better visualization, the recordings were filtered digitally with a 1 kHz low-pass filter. (ii) Data points showing the number of delivered DNA molecules per cycle. The orange solid line shows the average number of molecules delivered per cycle: 17.7 ± 4.5 molecules at $V^- = -400$ mV, 13.1 ± 3.3 molecules at $V^- = -300$ mV and 8.0 ± 3.0 molecules at $V^- = -200$ mV (mean value ± 1 standard deviation). (iii) Histogram showing the time distribution of the first event in a delivery cycle for the 24 delivery cycles. The first molecule is delivered faster at higher V^-.

delivery events for 10 kbp and 5 kbp DNA are available in Figure S1 in the Supporting Information). At 0.1 M KCl, the translocation of DNA through the tip of the nanopipet elicits a temporary increase in the conductance rather than a decrease. This effect is due to conducting counterions that shield the negatively charged phosphate backbone of the translocated DNA molecule, which has been observed before in similar ionic strength conditions.[24,33] The high reproducibility in the measured current between each delivery pulse can be used to combine single-molecule detection statistics from each pulse in all event histograms. Histograms and event scatter plots of peak current caused by translocations, ΔI *vs*. dwell time and equivalent charge (integrated current area per translocation) *vs*. dwell time are shown in Figure 2c, indicating that the most of

the DNA molecules are in an unfolded state when being translocated through the tip of the nanopipet.[12] This is also in agreement with the observation of translocation events as single steps in the ionic current as shown in Figure S1 in the Supporting Information. On the basis of calculations from the histogram fits, at $V^- = -300$ mV the most probable dwell time was 0.6 ± 0.2 ms with a mean equivalent charge of 18.0 ± 4.1 fAs. Both values are in good agreement with previously reported data for 10 kbp DNA molecules, albeit in those experiments DNA molecules were translocated from the external reservoir to the inside of the nanopipet.[26,27]

The reproducibility of the molecular delivery between individual pulses is illustrated in Figure 2d–f for $V^- = -200$ mV, -300 mV, and -400 mV, respectively. I–t traces of 15 representative V^- pulses (5 for each potential) are shown in panels (i) in Figure 2d–f, demonstrating a well-defined "time of arrival" dT, for the delivery of the first molecule in each V^- pulse, with a small spread in the delivery time of approximately the same magnitude as the average time between successive delivery events δt. Panels (ii) in Figure 2d–f show the number of molecules delivered per pulse for 24 consecutive pulses (total duration of 500 s). The average number of molecules delivered per pulse was 17.7 ± 4.5 at $V^- = -400$ mV, 13.1 ± 3.3 molecules at $V^- = -300$ mV and 8.0 ± 3.0 molecules at $V^- = -200$ mV. Panels (iii) illustrate the controllable delivery of the first molecule with a histogram of dT showing the distribution of the time of the first event. The first molecule is delivered faster for higher V; for 10 kbp DNA molecules with $t^+ = 6.4$ s and $V^+ = 500$ mV, the time of the first event dT was 2.9 ± 0.6 s, 3.8 ± 1.1 s, and 6.2 ± 0.9 s for $V^- = -400$ mV, -300 mV, and -200 mV, respectively. All error estimates are standard deviations. These results are not device-dependent in the sense that they have been reproduced with over 30 nanopipets fabricated with the same laser puller settings.

Experiment analogues to the ones shown in Figure 2 have been performed for 5 and 10 kbp DNA for a range of concentrations (3 pM to 1500 pM) and negative potentials V^- (-200 mV to -500 mV). Scatter plots and histograms showing delivery and detection of 5 kbp DNA molecules are available in Figure S2 in the Supporting Information. It was possible to reliably deliver and detect both 5 and 10 kbp DNA molecules from concentrations as low as 3 pM (equal to 3 amol of DNA sample in the nanopipet volume of ~ 1 μL), demonstrating the suitability of the method for the delivery and detection from ultrasmall sample volumes, without the need of amplification. These results indicate detection sensitivity that is directly comparable to ultralow concentration detection (3.8 pM DNA) only accomplished with high salt gradients across the nanopore.[4] Multiple single-molecule delivery data has been summarized in Figure S3 in the Supporting Information as measurements of 5 and 10 kbp DNA capture rates as a function of V^- at concentrations varying from 3 pM to 1500 pM. To avoid potential recapture of the already translocated DNA molecules,[34,35] a delay step of 0.6 s at 0 V was introduced between each delivery pulse (0.3 s before a V^+ pulse and after the V^- pulse). Gershow and Golovchenko have shown that the probability of recapture decreases dramatically with the time elapsed before the application of a reverse potential (V^+ here).[34] Indeed, recaptured DNA molecules were not observed in the V^+ current time traces as show in Figure S4 in the Supporting Information.

The transport of DNA through the nanopipet under pulsed potentials can in the first instance be described as the interplay of electrophoretic (EP) and electroosmotic (EO) forces, where DNA molecules are pulled back and forth along the nanopipet. For the current conditions the dominating force will be due to EP. In a V^+ pulse, the electroosmotic flow is directed from the inside to the outside of the nanopipet, while EP pulls DNA molecules that are already close to the tip toward the nanopipet interior. The DNA molecules, which are initially randomly distributed inside the nanopipet, (except very close to the tip (~ 2 μm), where they are excluded, due to sterical restraints), get pulled along the nanopipet axis to a distance z from the tip, depending on the duration of the positive pulse (t^+). When a negative pulse V^- is applied (at the time $t = t^+$) the electroosmotic flow is directed into the nanopipet, while EP moves the DNA molecules toward the nanopore. For negative pulses with sufficiently long duration ($t^- >$ dT), the DNA molecules have enough time to travel the distance z to the nanopore followed by delivery. This mechanism is the basis of the controllable delivery and was confirmed by fluorescence imaging of labeled DNA at the nanopipet tip (Figure 3, Figure S5 and the movie in the Supporting Information) and finite element simulations (Figure S6 in the Supporting Information), in addition to the presented ionic current data.

To estimate the rate of transport of DNA in the nanopipet, the following approximate expression is used:

$$C_R = \frac{\mu_{ep} I}{K} C + Q_{eo} C \qquad (1)$$

where C_R is the average number of DNA molecules passing a cross-section of the nanopipet per second (equal to the average capture rate at the nanopore), C is the concentration of DNA in the nanopipet, μ_{ep} is the electrophoretic mobility of the DNA, I is the ion current, K the (bulk) ion conductivity, and Q_{eo} the electroosmotic flow. This expression is based on the assumption of having, on average, the same amount of DNA molecules passing each cross section of the nanopipet. This is the equivalent of having no local accumulation

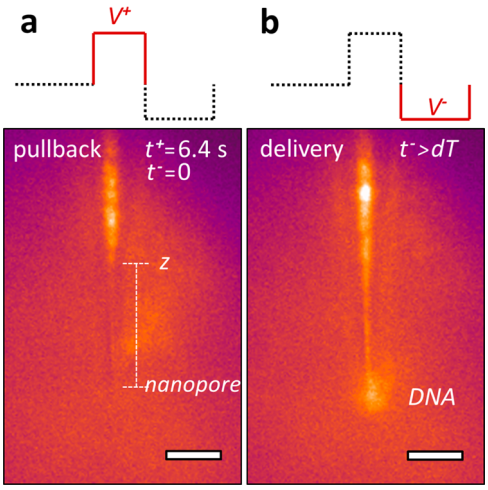

Figure 3. Fluorescence imaging of DNA molecules at the nanopipet tip. (a) Image of the tip at the end of a positive pulse (at t^+ = 6.4 s) at $V = V^+ = 500$ mV, showing tip depletion of the DNA molecules to a position z from the tip of the nanopipet. In repeating pulse cycles, the DNA molecules were pulled to the same position z (additional information is available in Figures S5 and S9 in the Supporting Information). (b) Image of the tip at $V = V^- = -300$ mV at $t^- = 5$ s ($t = 11.4$ s), DNA is delivered through the nanopore at the tip of the nanopipet. The DNA sample was 1500 pM, 10 kbp, labeled with YOYO-1 fluorescent dye. All scale bars are 10 μm. A movie demonstrating the delivery process is available in the Supporting Information.

or depletion of DNA molecules in the nanopipet, an assumption that is supported by fluorescence imaging of DNA in the nanopipet (Figure 3). Even if the concentration of ions close to the tip of the nanopipet is changing under conditions of ion rectification, the concentration far from the tip should be independent of the sign of the applied voltage[36,37] and the electric field in that region can be estimated by $I/(A \times K)$, where A is the cross-sectional area of the nanopipet in the studied region. The exact values of the terms in eq 1 close to the tip might be different, and other forces such as dielectrophoresis might also act on the DNA molecules in this region,[38] but since the transport of the DNA molecules is mainly taking place in the region far from the tip (see Figure S8 and movie in the Supporting Information) this effect can be neglected for the current experiments.

Finite element simulations were performed in COMSOL Multiphysics 4.3b to estimate I and Q_{eo} under different applied voltages (cf. the Methods section and Figures S6 and S7 in the Supporting Information) for the same nanopipet geometry as measured optically and by SEM. The time to the first event, dT, can, as a first approximation, be estimated by the following expression (see the Supporting Information for details):

$$\mathrm{dT} = -\frac{(\mu_{ep} I_+ + KQ_{eo,+})}{(\mu_{ep} I_- + KQ_{eo,-})} t^+ \qquad (2)$$

where the $\pm$ signs indicate the ion current and the electroosmotic flow rate for the positive/negative pulses. Inserting the simulated values for the ion current and the electroosmotic flow (Figure S6b,c in the Supporting Information) gives dT as a function of V^-, V^+ and t^+ only. Figure 4a shows experimentally measured dT for different V^- (for $V^+ = 500$ mV and $t^+ = 6.4$ s) based on 643 delivery cycles for 5 kbp and 10 kbp DNA molecules with a concentration of 30 pM and 150 pM. The experimentally measured dT values were found to be in relatively good agreement with the estimated values from eq 2 (dashed lines in Figure 4a), showing an increase in the delivery time with lower voltages V^- due to a lower flux of DNA in the nanopipet. However, eq 2 does not describe the dependency of dT with the concentration of DNA in the nanopipet and the length of the DNA molecules, which from Figure 4a is seen to have an effect on the delivery time. To investigate this and to estimate the spread in the delivery times, we performed time-dependent finite elements simulations of the delivery during a voltage cycle (for details see the Methods section and Figure S8 in the Supporting Information). The results of these simulations are shown as solid lines in Figure 4a (and Figure 4c) and are in good agreement with the experimental values. The average delivery time decreases when the concentration of DNA molecules increases (Figure 4a). An explanation to this behavior is that, due to the random distribution of DNA molecules in the nanopipet at $t = 0$, the DNA molecule closest to the tip of the nanopipet is on average further away from the tip at $t = 0$ for lower concentrations compared to higher concentrations. These DNA molecules will therefore travel further into the nanopipet during the positive voltage pulse and will exit the nanopipet at a later time dT (see also Figure S9 in the Supporting Information). There will also be a higher likelihood of a DNA molecule having diffused (a longer distance) toward the tip of the nanopipet when the concentration is increased, thus resulting in a lower dT. This will also be affected by the diffusivity of the molecule, which is why shorter (5 kbp) DNA molecules have slightly lower dT than the longer (10 kbp) DNA molecules (see Figure 4a).

The time of delivery can also be adjusted by varying the positive pulse duration t^+. Figure 4b provides a plot of dT values measured in 340 delivery cycles with $V^+ = 500$ mV, $V^- = -300$ mV, and $t^- = 21$ s as a function of t^+ together with data from the time-dependent simulations, showing an excellent agreement between experimental and simulated data. The value for dT is initially increasing linearly with t^+ as predicted from eq 2, in agreement between the measured slope ($\mathrm{dT}/t^+ = 0.69 \pm 0.03$) and the one calculated from eq 2 ($\mathrm{dT}/t^+ = 0.71$). The delivery time is decreasing at higher t^+ due to increased diffusion when the DNA is transported further into the nanopipet. In summary, both the theoretical and experimental results demonstrate that, for a constant value of V^-, the precise time of the

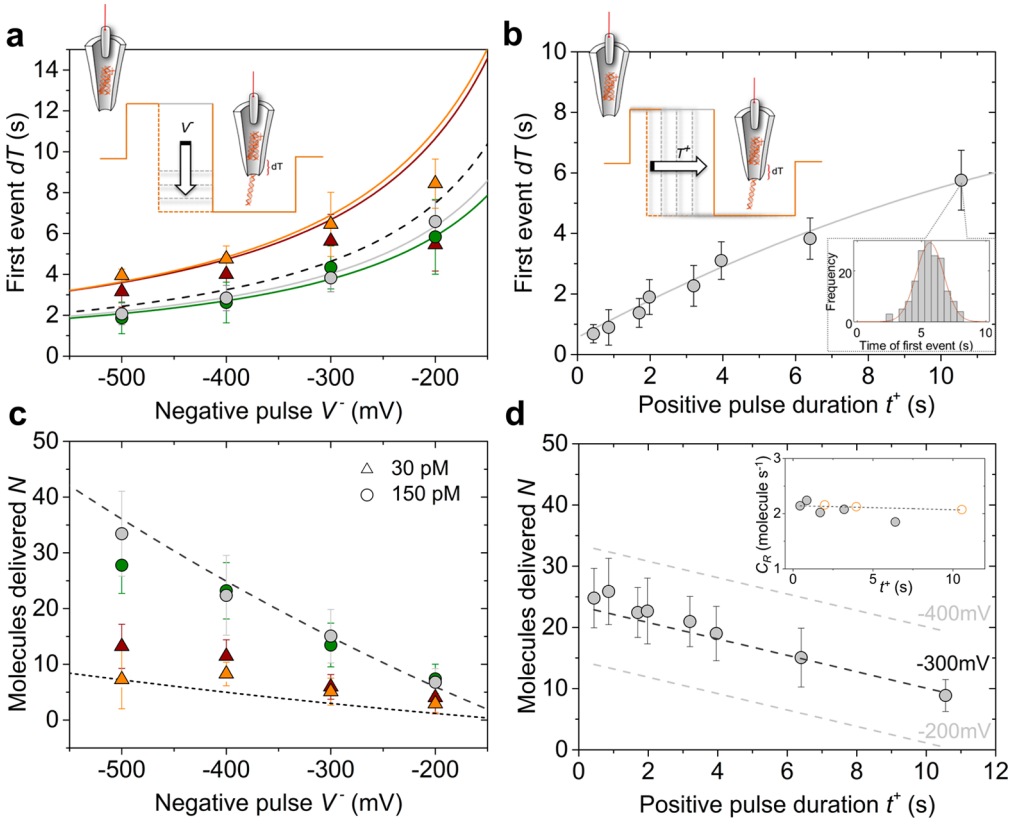

Figure 4. Controllable delivery of DNA molecules. The time of the first event dT and the number of molecules delivered in a pulse is accurately controlled by varying the potentials V^+ and V^- and the positive pulse duration t^+. (a) Experimentally measured times of the first event as a function of the applied potential V^- for 356 delivery pulses of 30 pM 10 kbp (orange triangles), 30 pM 5 kbp (red triangles), 150 pM 10 kbp (gray circles), and 150 pM 5 kbp DNA (green circles). The curves show theoretical values of dT from either time-dependent simulations (solid lines; color coded the same as the experimental data) and from eq 2 (dashed line). Both experiments and simulations have been carried out for positive pulses, $V^+ = 500$ mV and $t^+ = 6.4$ s. (b) Time of the first event as a function of t^+ for 150 pM 10 kbp DNA, with $V^+ = 500$ mV and $V^- = -300$ mV. The solid line shows the predicted values of dT from time-dependent finite element simulations. The inset shows a histogram for the last data point ($t^+ = 10.6$ s) based on 168 consecutive measurements of dT. A total number of 5501 DNA molecules were delivered over 5700 s. (c) Number of molecules, N, delivered in a negative pulse with a fixed duration ($t^- = 12.7$ s) for different negative pulse potentials V^- of 30 pM 10 kbp (orange triangles), 30 pM 5 kbp (red triangles), 150 pM 10 kbp (gray circles), and 150 pM 5 kbp DNA (green circles), with predicted values of dT from eq 3, using eq 2 for dT, (dashed lines). (d) Number of delivered molecules per pulse ($t^- = 12.7$ s) for different positive pulse durations t^+ ($V^+ = 500$ mV and $V^- = -300$ mV). (inset) DNA capture rate measurements for different positive pulse durations t^+ for $t^- = 12.7$ s (gray circles) and $t^- = 21.0$ s (orange circles). The dashed lines are theoretical values from eq 3 using eq 2 to calculate dT.

delivery of the first molecule can be controlled by the duration of the positive potential t^+. While molecular delivery occurs when negative pulses are applied, decreasing the duration of the positive pulse t^+ results in quicker delivery of the first molecule.

The number of DNA molecules delivered per pulse, N, is given by

$$N = C_R(t^- - \mathrm{dT}) \qquad (3)$$

Together with eqs 1 and 2, the number of molecules delivered in a negative pulse with a set duration t^- is proportional to the analyte concentration C. The number of delivered molecules can be controlled by varying dT, V^- (see Figure 4c), V^+ or t^+ (see Figure 4d). Figure 4c shows that varying V^- has two effects: (i) an increase of V^- results in a higher capture rate C_R (see eq 1) thus increasing the number of DNA molecules delivered and (ii) an increase in V^- reduces the time dT thus leading to a larger time ($t^- - \mathrm{dT}$) for delivery and more DNA molecules being delivered. Figure 4d shows the variation of the number of delivered DNA molecules with different values of t^+. Since C_R is independent of t^+ (and t^-), as measured experimentally and shown in the inset in Figure 4d, the only time dependence in N is in the term ($t^- - \mathrm{dT}$) (see eq 3). Since dT is proportional to t^+ (as indicated by eq 2 and experimentally shown in Figure 4b), the total number of delivered molecules will also decrease linearly with t^+ as shown in the experimental and the theoretical data in Figure 4d.

These findings further confirm that during alternating pulses DNA molecules are transported back and forth close to the nanopipet tip and demonstrate that the potentials V^+ and V^-, as well as the pulse duration t^+, can be used to actively control the delivery of a defined number of DNA molecules. The control over dT

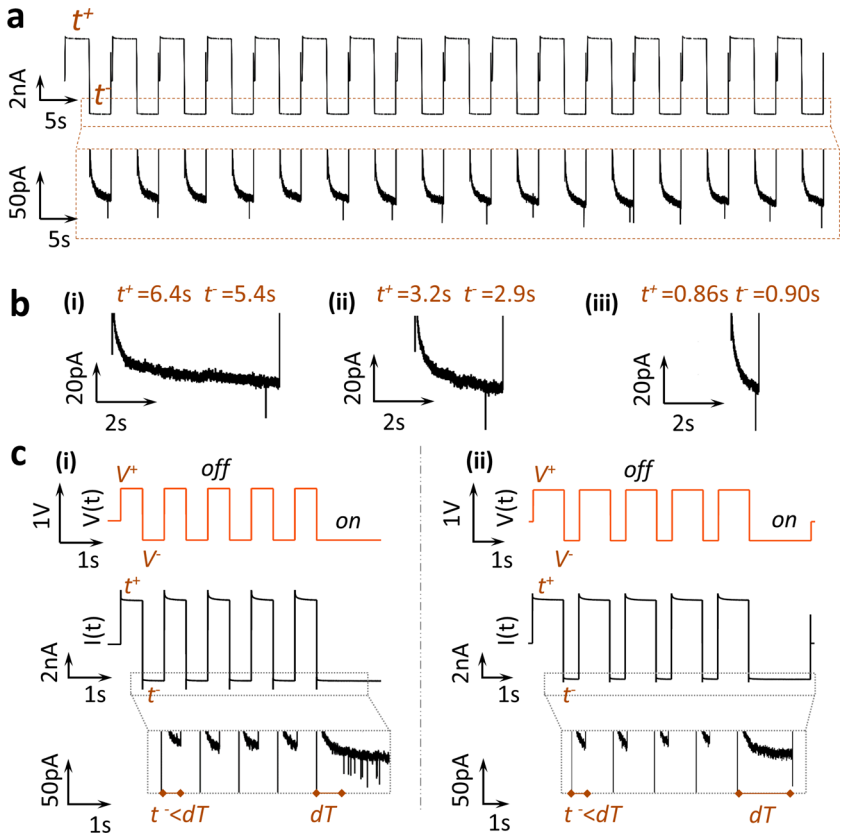

Figure 5. Delivery of single DNA molecules. (a) $I-t$ trace showing 16 consecutive pulses (100 s in total) illustrating delivery of single DNA molecules (top panel) and a blow up of the events (lower panel) for 1500 pM 10 kbp DNA with $V^+ = 500$ mV, $V^- = -300$ mV, $t^+ = 3.2$ s, and $t^- = 2.9$ s. (b) Representative $I-t$ pulses for different t^+ and t^- combinations, showing single molecule delivery in a pulse. Single molecules are delivered faster by using short t^+. (c) Switching molecular delivery "on and off" on demand. Measured $V-t$ and $I-t$ pulses for 1500 pM, 10 kbp DNA with $V^+ = 500$ mV and $V^- = -300$ mV. The bottom panel shows the blown up $I-t$ trace. DNA molecules are pulsed back and forth in the nanopipet close to the tip opening without being delivered when operated in the regime $t^- < dT$ (first four cycles). Molecular delivery is then achieved on-demand by switching to $t^- > dT$. (c_i) Multiple molecules are delivered on demand and (c_{ii}) single molecule delivered in a pulse.

can further be used for the precise delivery of individual molecules in a single pulse. The negative pulse duration t^- can be set such that on average only one molecule is delivered in a pulse (as shown in several consecutive pulses in Figure 5a). The latter is also demonstrated in Figure 5b_i to b_{iii} for three different combinations of t^+ and t^- (with up to 75 delivery pulses each), chosen for values of dT such that $N = 1$ as predicted from the time-dependent simulations and from eqs 2 and 3. It should be noted that prior to applying voltage pulses, the DNA molecules are randomly distributed in the nanopipet and the probability density function of finding a DNA molecule is assumed to be the same at all position in the nanopipet. This will not be true close to the tip of the nanopipet (within $\sim 2\ \mu$m from the tip), where in the absence of voltage pulses, the DNA molecules will be excluded due to sterical constraints. Since the DNA molecules for the majority of the delivery cycle are further away than this distance, this can be used as a first approximation. From the random distribution of DNA in the nanopipet at $t = 0$, it is thus expected that the delivery should also contain a spread in dT and that the number of molecules being delivered after a time t^- should follow a Poisson distribution. Comparing experimental results versus simulated predictions based on Poisson statistics for the number of molecules delivered per cycle for different combinations of t^+ and t^- generally shows good agreement, which states a maximum likelihood of one DNA molecule being delivered of $1/e \approx 0.37$. However, it should be mentioned that delivery situations also occur, which are very unlikely based on Poisson statics. An example of this deviation is shown in Figure 5a where 13 single molecule delivery events out of 16 consecutive pulses are observed. The likelihood of this occurring is less than 1 in 5000. It is thus possible that other effects, such as confinement or steric exclusion at and near the tip of the nanopipet, can affect the delivery, resulting in a higher likelihood of getting a single delivery event than expected from Poisson statistics.

Since dT is proportional to t^+, it is possible to deliver single molecules in a short pulse with a low dT, just by varying t^+ (as can be seen from the pulse durations in Figure 5b). Additional experimental data (plots of dT distribution and the number of molecules delivered

per cycle) for a constant t^+ (hence a constant dT), showing, as predicted, an increase of the number of molecules delivered per cycle with increasing t^-, are available in Figure S10 in the Supporting Information.

The control over dT can further be used in the regime $t^- < dT$, to repeatedly pulse molecules in the nanopipet, back and forth close to the nanopore, without delivering the molecule. Molecular delivery can thus be switched on-demand for $t^- > dT$, to deliver a specific number of molecules (Figure 5c$_i$) or a single molecule by controlling dT (Figure 5c$_{ii}$). In principle, the experimental regimes presented in Figure 5a,c$_{ii}$ can be combined to alternate between pulsing a molecule close to the tip and on-demand delivery of a single molecule. This unique capabilities of on-demand, switchable molecular delivery and simultaneous label-free detection can serve as a particularly powerful tool in studies with living cells. The nanopipets used in this work can be integrated with ion conductance microscopy to scan ($t^- < dT$) the surface of living cells and perform targeted delivery on demand ($t^- > dT$) in a cell area of choice. Another exciting application is the possibility of using the region inside the nanopipet, near the tip as an ultrasmall reaction volume,[39] where small molecular populations are pulsed back and forth and interact with each other, with the reaction products simultaneously delivered and detected by the nanopore.

CONCLUSIONS

In this article we showed controllable delivery of single DNA molecules with simultaneous label-free detection. We demonstrated that even highly diluted unamplified molecular populations can be efficiently delivered with control of the time of delivery of the first molecule and the number of molecules delivered. We believe that these findings can open the door to using nanopipets as a single molecule delivery tool, which is expected to have a broad range of applications, including targeted delivery of nucleic acids, gene regulation, infection, and single molecule PCR.

METHODS

Nanopipet Fabrication. Nanopipets were fabricated using a P-2000 laser puller (Sutter Instrument Co) from quartz capillaries with an outer diameter of 1.0 mm and an inner diameter of 0.5 mm (QF100-50-7.5; Sutter Instrument Co).

Nanopipets were fabricated using a two-line protocol: (1) HEAT, 575; FIL, 3; VEL, 35; DEL, 145; PUL, 75, followed by (2) HEAT, 900; FIL, 2; VEL, 15; DEL, 128; PUL, 200. It should be noted that the pulling protocol is instrument specific and there is variation between P-2000 pullers.

DNA Solutions. Double stranded DNA with lengths 5 kbp and 10 kbp and with a stock concentration of 500 μg/mL were obtained from New England Biolabs. DNA filling solutions (3 pM, 30 pM, 150 pM, and 1500 pM) were prepared by serial dilution. The filling concentrations were cross-checked with a NanoDrop 2000c UV−vis spectrophotometer (Thermo Fisher Scientific Inc.). Each nanopipet was filled once and used with only one solution. Nanopipets once used in an experiment were not reused.

Finite Element Simulations. Finite element simulations were performed in COMSOL Multiphysics 4.3b (COMSOL AB) to model the electric field, the ion current, and the electroosmotic flow in a nanopipet with $R_0 = 12$ nm, $\theta = 3.5°$, and $R_1 = 2R_0$. Similar simulations have previously been done for nanopores[36,37] and for nanopipets.[31] The geometry used for the simulations is shown in Figure S6 in the Supporting Information. The surface charge of the nanopipet walls, σ, was estimated for 0.1 M KCl (conductivity of $K \approx 1.5$ S/m) as

$$\sigma = \kappa \varepsilon_r \varepsilon_0 \zeta \quad (4)$$

where κ is the inverse Debye length, ε_r the relative permittivity of the solution, ε_0 the permittivity of vacuum, and ζ the zeta potential of the nanopipet walls. The zeta potential for glass in a 0.1 M K^+ solution is approximately −30 mV (see ref 40) resulting in a surface charge of −22 mC/m^2. COMSOL Multiphysics was also used to solve the time-dependent diffusion/transport equation to in detail model the transport of DNA back and forth in the nanopipet during a voltage cycle (see Figures S6 and S7 in the Supporting Information for the simulation geometry). The nanopipet was assumed to be homogeneously filled with DNA molecules at $t = 0$ and thus that the probability density function, c, of finding the DNA was the same at any position in the nanopipet. The distribution of c was then determined at subsequent times, and the molecular flux of DNA out of the nanopipet was calculated and used to determine the time of delivery of a single DNA molecule and the delivery probability. Further details on the simulations are given in the Supporting Information together with theoretical formulas of how the simulated data was converted into values of dT and delivery probabilities.

Ionic Current Detection. The ion current was measured using a MultiClamp 700B or AxoPatch 200B patch-clamp amplifier (Molecular Devices) in "voltage clamp" mode. The signal was filtered using a low-pass filter at 10 kHz and digitized with an Axon Digidata 1322A or Digidata 1440 at a 50 kHz rate and recorded using the software pClamp 8/10 (Molecular Devices). Data analysis was carried out using a custom-written MATLAB analysis routine. The baseline current was calculated via moving window for every 5 data points. Peak current was calculated as current peak maximum after subtraction of the baseline current.

Fluorescence Detection. The DNA stock solutions were labeled with YOYO-1 (Molecular Probes) at a ratio of 7.5 base pairs per dye molecule. Detection of DNA was achieved using a custom-built confocal microscope with imaging capabilities.[41,42] Briefly, the excitation light from a 488 nm continuous wave laser was expanded on the nanopipet tip using a 60× objective). Fluorescence originating from DNA molecules transported along the tip and translocating through the nanopore was collected by the same objective and directed to an electron multiplying CCD (emCCD) camera (Cascade II, Photometrics). The camera has a pixel size of 16 μm, however, when used in conjunction with the 60× objective, generates an effective pixel size of 266 nm.

Conflict of Interest: The authors declare no competing financial interest.

Acknowledgment. J.B.E. has been funded in part by an ERC starting investigator grant and a BBSRC grant. P.J. was supported by a grant from the Swedish Research Council (Number 623-2014-6387).

Supporting Information Available: Finite element simulations of the ion current and the electroosmotic flow, finite element simulations of a voltage cycle, theoretical expressions describing the delivery, and a movie demonstrating the delivery process. This material is available free of charge via the Internet at http://pubs.acs.org.

REFERENCES AND NOTES

1. Dekker, C. Solid-State Nanopores. *Nat. Nanotechnol.* **2007**, *2*, 209–215.

2. Venkatesan, B. M.; Bashir, R. Nanopore Sensors for Nucleic Acid Analysis. *Nat. Nanotechnol.* **2011**, *6*, 615–624.
3. Miles, B. N.; Ivanov, A. P.; Wilson, K. A.; Dogan, F.; Japrung, D.; Edel, J. B. Single Molecule Sensing with Solid-State Nanopores: Novel Materials, Methods, and Applications. *Chem. Soc. Rev.* **2013**, *42*, 15–28.
4. Wanunu, M.; Morrison, W.; Rabin, Y.; Grosberg, A. Y.; Meller, A. Electrostatic Focusing of Unlabelled DNA into Nanoscale Pores Using a Salt Gradient. *Nat. Nanotechnol.* **2010**, *5*, 160–165.
5. Ivanov, A. P.; Instuli, E.; McGilvery, C. M.; Baldwin, G.; McComb, D. W.; Albrecht, T.; Edel, J. B. DNA Tunneling Detector Embedded in a Nanopore. *Nano Lett.* **2010**, *11*, 279–285.
6. Wei, R.; Gatterdam, V.; Wieneke, R.; Tampe, R.; Rant, U. Stochastic Sensing of Proteins with Receptor-Modified Solid-State Nanopores. *Nat. Nanotechnol.* **2012**, *7*, 257–263.
7. Storm, A. J.; Storm, C.; Chen, J. H.; Zandbergen, H.; Joanny, J. F.; Dekker, C. Fast DNA Translocation Through a Solid-State Nanopore. *Nano Lett.* **2005**, *5*, 1193–1197.
8. Iqbal, S. M.; Akin, D.; Bashir, R. Solid-State Nanopore Channels with DNA Selectivity. *Nat. Nanotechnol.* **2007**, *2*, 243–248.
9. Wanunu, M.; Bhattacharya, S.; Xie, Y.; Tor, Y.; Aksimentiev, A.; Drndic, M. Nanopore Analysis of Individual RNA/Antibiotic Complexes. *ACS Nano* **2011**, *5*, 9345–9353.
10. Li, W.; Bell, N. A. W.; Hernandez-Ainsa, S.; Thacker, V. V.; Thackray, A. M.; Bujdoso, R.; Keyser, U. F. Single Protein Molecule Detection by Glass Nanopores. *ACS Nano* **2013**, *7*, 4129–4134.
11. Karhanek, M.; Kemp, J. T.; Pourmand, N.; Davis, R. W.; Webb, C. D. Single DNA Molecule Detection Using Nanopipettes and Nanoparticles. *Nano Lett.* **2005**, *5*, 403–407.
12. Steinbock, L. J.; Otto, O.; Chimerel, C.; Gornall, J.; Keyser, U. F. Detecting DNA Folding with Nanocapillaries. *Nano Lett.* **2010**, *10*, 2493–2497.
13. Li, W.; Bell, N. A. W.; Hernández-Ainsa, S.; Thacker, V. V.; Thackray, A. M.; Bujdoso, R.; Keyser, U. F. Single Protein Molecule Detection by Glass Nanopores. *ACS Nano* **2013**, *7*, 4129–4134.
14. Haywood, D. G.; Saha-Shah, A.; Baker, L. A.; Jacobson, S. C. Fundamental Studies of Nanofluidics: Nanopores, Nanochannels, and Nanopipets. *Anal. Chem.* **2015**, *87*, 172–187.
15. Novak, P.; Li, C.; Shevchuk, A. I.; Stepanyan, R.; Caldwell, M.; Hughes, S.; Smart, T. G.; Gorelik, J.; Ostanin, V. P.; Lab, M. J.; et al. Nanoscale Live-Cell Imaging Using Hopping Probe Ion Conductance Microscopy. *Nat. Methods* **2009**, *6*, 279–281.
16. Actis, P.; Tokar, S.; Clausmeyer, J.; Babakinejad, B.; Mikhaleva, S.; Cornut, R.; Takahashi, Y.; Cordoba, A. L.; Novak, P.; Shevchuck, A. I.; et al. Electrochemical Nanoprobes for Single-Cell Analysis. *ACS Nano* **2014**, *8*, 875–884.
17. Knoblauch, M.; Hibberd, J. M.; Gray, J. C.; van Bel, A. J. E. A Galinstan Expansion Femtosyringe for Microinjection of Eukaryotic Organelles and Prokaryotes. *Nat. Biotechnol.* **1999**, *17*, 906–909.
18. Bruckbauer, A.; James, P.; Zhou, D. J.; Yoon, J. W.; Excell, D.; Korchev, Y.; Jones, R.; Klenerman, D. Nanopipette Delivery of Individual Molecules to Cellular Compartments for Single-Molecule Fluorescence Tracking. *Biophys. J.* **2007**, *93*, 3120–3131.
19. Singhal, R.; Orynbayeva, Z.; Sundaram, R. V. K.; Niu, J. J.; Bhattacharyya, S.; Vitol, E. A.; Schrlau, M. G.; Papazoglou, E. S.; Friedman, G.; Gogotsi, Y. Multifunctional Carbon-Nanotube Cellular Endoscopes. *Nat. Nanotechnol.* **2011**, *6*, 57–64.
20. Adam Seger, R.; Actis, P.; Penfold, C.; Maalouf, M.; Vilozny, B.; Pourmand, N. Voltage Controlled Nano-Injection System For Single-Cell Surgery. *Nanoscale* **2012**, *4*, 5843–5846.
21. Babakinejad, B.; Jönsson, P.; López Córdoba, A.; Actis, P.; Novak, P.; Takahashi, Y.; Shevchuk, A.; Anand, U.; Anand, P.; Drews, A.; et al. Local Delivery of Molecules from a Nanopipette for Quantitative Receptor Mapping on Live Cells. *Anal. Chem.* **2013**, *85*, 9333–9342.
22. Actis, P.; Maalouf, M. M.; Kim, H. J.; Lohith, A.; Vilozny, B.; Seger, R. A.; Pourmand, N. Compartmental genomics in living cells revealed by single-cell nanobiopsy. *ACS Nano* **2014**, *8*, 546–553.
23. Ying, L.; Bruckbauer, A.; Rothery, A. M.; Korchev, Y. E.; Klenerman, D. Programmable Delivery of DNA through a Nanopipet. *Anal. Chem.* **2002**, *74*, 1380–1385.
24. Steinbock, L. J.; Lucas, A.; Otto, O.; Keyser, U. F. Voltage-Driven Transport of Ions and DNA through Nanocapillaries. *Electrophoresis* **2012**, *33*, 3480–3487.
25. Bell, N. A.; Thacker, V. V.; Hernandez-Ainsa, S.; Fuentes-Perez, M. E.; Moreno-Herrero, F.; Liedl, T.; Keyser, U. F. Multiplexed Ionic Current Sensing with Glass Nanopores. *Lab Chip* **2013**, *13*, 1859–1862.
26. Gong, X.; Patil, A. V.; Ivanov, A. P.; Kong, Q.; Gibb, T.; Dogan, F.; deMello, A. J.; Edel, J. B. Label-Free In-Flow Detection of Single DNA Molecules Using Glass Nanopipettes. *Anal. Chem.* **2014**, *86*, 835–841.
27. Gibb, T. R.; Ivanov, A. P.; Edel, J. B.; Albrecht, T. Single Molecule Ionic Current Sensing in Segmented Flow Microfluidics. *Anal. Chem.* **2014**, *86*, 1864–1871.
28. Wei, C.; Bard, A. J.; Feldberg, S. W. Current Rectification at Quartz Nanopipet Electrodes. *Anal. Chem.* **1997**, *69*, 4627–4633.
29. Siwy, Z.; Fulinski, A. Fabrication of a Synthetic Nanopore Ion Pump. *Phys. Rev. Lett.* **2002**, *89*, 198103.
30. Lan, W.-J.; Holden, D. A.; White, H. S. Pressure-Dependent Ion Current Rectification in Conical-Shaped Glass Nanopores. *J. Am. Chem. Soc.* **2011**, *133*, 13300–13303.
31. Sa, N.; Baker, L. A. Experiment and Simulation of Ion Transport through Nanopipettes of Well-Defined Conical Geometry. *J. Electrochem. Soc.* **2013**, *160*, 376–381.
32. Freedman, K. J.; Haq, S. R.; Fletcher, M. R.; Foley, J. P.; Jemth, P.; Edel, J. B.; Kim, M. J. Nonequilibrium Capture Rates Induce Protein Accumulation and Enhanced Adsorption to Solid-State Nanopores. *ACS Nano* **2014**, *8*, 12238–12249.
33. Smeets, R. M. M.; Keyser, U. F.; Krapf, D.; Wu, M.-Y.; Dekker, N. H.; Dekker, C. Salt Dependence of Ion Transport and DNA Translocation through Solid-State Nanopores. *Nano Lett.* **2005**, *6*, 89–95.
34. Gershow, M.; Golovchenko, J. A. Recapturing and trapping single molecules with a solid-state nanopore. *Nat. Nanotechnol.* **2007**, *2*, 775–779.
35. Plesa, C.; Cornelissen, L.; Tuijtel, M. W.; Dekker, C. Non-Equilibrium Folding of Individual DNA Molecules Recaptured up to 1000 Times in a Solid State Nanopore. *Nanotechnology* **2013**, *24*, 475101.
36. Kubeil, C.; Bund, A. The Role of Nanopore Geometry for the Rectification of Ionic Currents. *J. Phys. Chem. C* **2011**, *115*, 7866–7873.
37. White, H. S.; Bund, A. Ion current rectification at nanopores in glass membranes. *Langmuir* **2008**, *24*, 2212–2218.
38. Ying, L.; White, S. S.; Bruckbauer, A.; Meadows, L.; Korchev, Y. E.; Klenerman, D. Frequency and Voltage Dependence of the Dielectrophoretic Trapping of Short Lengths of DNA and dCTP in a Nanopipette. *Biophys. J.* **2004**, *86*, 1018–1027.
39. Bruckbauer, A.; Zhou, D. J.; Ying, L. M.; Abell, C.; Klenerman, D. A Simple Voltage Controlled Enzymatic Nanoreactor Produced in the Tip of a Nanopipet. *Nano Lett.* **2004**, *4*, 1859–1862.
40. Kirby, B. J.; Hasselbrink, E. F., Jr. Zeta potential of microfluidic substrates: 1. Theory, experimental techniques, and effects on separations. *Electrophoresis* **2004**, *25*, 187–202.
41. Chansin, G. A. T.; Mulero, R.; Hong, J.; Kim, M. J.; Demello, A. J.; Edel, J. B. Single-Molecule Spectroscopy Using Nanoporous Membranes. *Nano Lett.* **2007**, *7*, 2901–2906.
42. Cecchini, M. P.; Wiener, A.; Turek, V. A.; Chon, H.; Lee, S.; Ivanov, A. P.; McComb, D. W.; Choo, J.; Albrecht, T.; Maier, S. A.; et al. Rapid Ultrasensitive Single Particle Surface-Enhanced Raman Spectroscopy Using Metallic Nanopores. *Nano Lett.* **2013**, *13*, 4602–4609.